Some Aspects of Cloud and Precipitation Features Associated with a Mid-Latitude Cyclone

ELFORD G. ASTLING

Department of Meteorology, University of Utah, Salt Lake City, Utah 84112

(Manuscript received 29 June 1976, in revised form 13 September 1976)

ABSTRACT

A multi-level diagnostic model is used to study the physical and dynamical mechanisms that produce low-level clouds and light precipitation within the cold air sector on the west side of a Midwest cyclone. Computational results show frictional effects to be the primary mechanism in the absence of secondary upper level trough mechanisms or intense heating from the underlying surface. Also, this study shows that the vertical motion field may be substantially modified by secondary effects when the usually dominant contributions by vorticity and thermal effects are weak.

1. Introduction

This paper presents some results of a diagnostic study of a mid-latitude cyclone. In particular, attention is focused on mechanisms that produce low-level clouds and precipitation within the cold-air sector to the west of a cyclone center. Often the weather in this portion of the cyclone is characterized by low, overcast clouds and very light precipitation. Many intense wintertime cyclones exhibit this feature, especially over continental areas. Excellent examples have been documented by Anderson and Veltishchev (1973) with visible and infrared satellite data. Visible imagery shows the horizontal cloud distribution, while infrared imagery provides information about the vertical extent of the cloud field.

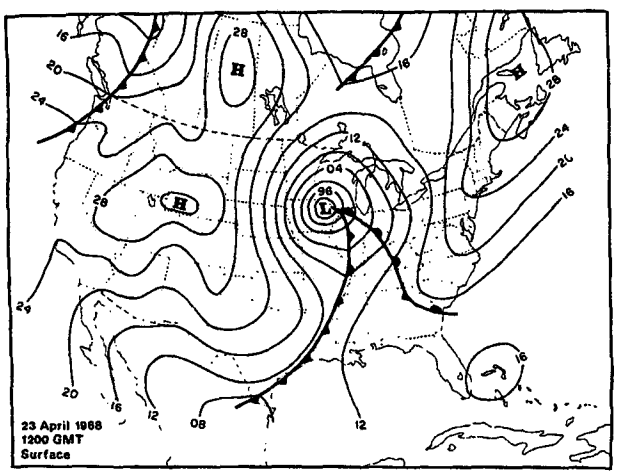

FIG. 1. Sea level pressure (mb) for 1200 GMT on 23 April 1968.

The weather in the west sector of the cyclone is not very dramatic compared to the mesoscale convective systems that are sometimes found ahead of the cold front. However, the low-level overcast cloud pattern is associated with cyclones throughout the wintertime and presents a forecast problem because the classical sequence of weather events does not occur (Astling, 1976). That is, with a cyclone moving eastward to the north of a station, the cold front passage is followed by only a brief period of dissipating clouds and rapid clearing before overcast skies return. Obviously, this problem is important in forecasting aviation weather and, more recently, in forecasting available solar radiation for energy related studies.

The clouds and precipitation may be explained by a number of physical mechanisms. In some cases the weather may be associated with short-wave troughs that move into a system from the upstream side of the major trough associated with the cyclone. In other situations orographic effects are responsible. This is particularly true for the eastern United States where orographic lifting due to the Appalachian Mountains, although weak compared to the influence of the Rocky Mountains, is a very likely mechanism (Colucci, 1976). For other systems the heat and moisture source provided by the Great Lakes during the winter are important factors.

2. Weather and cloud fields

The cyclone examined in this investigation was present over the Midwest at 1200 GMT 23 April 1968. Fig. 1 shows the sea level pressure distribution and surface fronts, while Fig. 2 illustrates the 500 mb height and temperature fields. This cyclone exhibited a slight

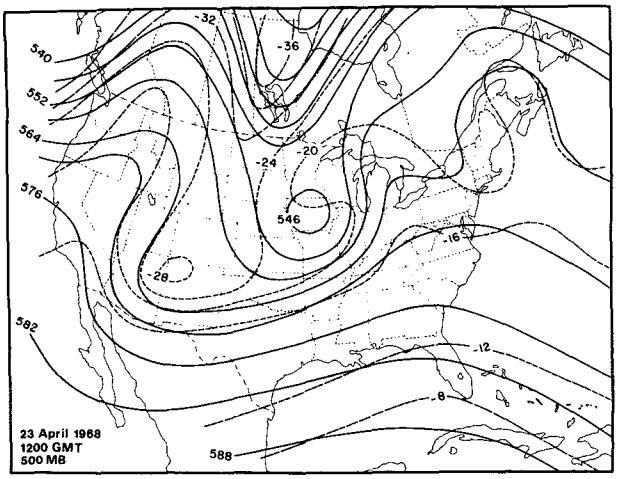

FIG. 2. Map of the 500 mb level. Solid lines represent contour heights (dam) and dashed lines isotherms (°C).

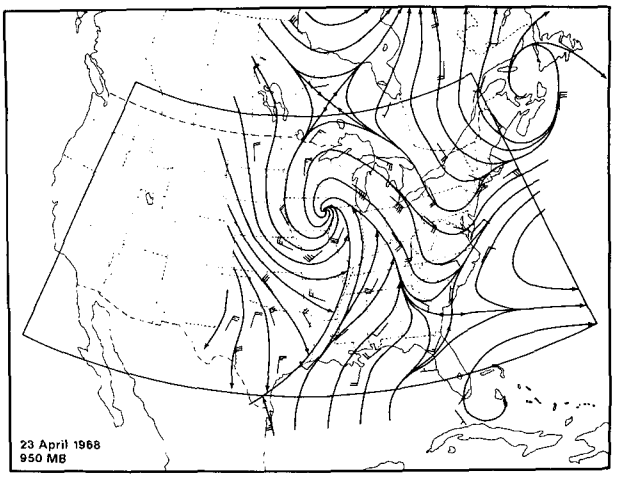

FIG. 4. Streamline analysis of the 950 mb level. Full barb = 10 kt.

vertical tilt toward the west with height and was accompanied by an extensive low-level cloud and precipitation area to the west of the surface cyclone center as depicted in Fig. 3. Conventional synoptic observations and radar summaries over southwestern Minnesota and Iowa revealed the presence of light continuous precipitation, and this weather represented the important features considered in this study. Hourly precipitation amounts reported at stations in this area were less than 0.05 inch for the map time shown in Fig. 1. Rainfall intensities ahead of the cold front were greater than 0.15 inch h^{-1} and produced 24 h accumulations of more than 1 inch in Iowa and Missouri before the frontal passage. Radiosonde observations at St. Cloud, Minn., and Omaha, Nebr., indicated a moist layer was present beneath a pronounced inversion at 700 mb and several synoptic observations reported stratus clouds.

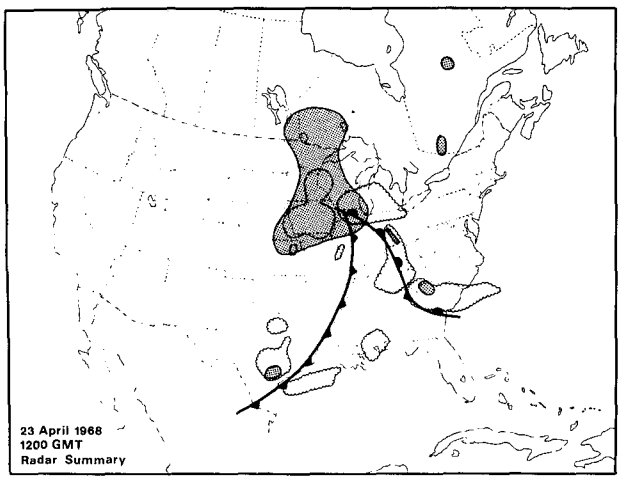

FIG. 3. Radar summary and precipitation distribution. Areas depicted with scalloped lines represent radar echoes at 1135 GMT. Stippled areas denote precipitation from 1200 GMT synoptic observations.

The lower and mid-tropospheric wind fields are represented by streamline analysis in Figs. 4 and 5. These analyses show some important subtle features in the wind field that are not easily identified in Figs. 1 and 2. The most notable feature was the northerly confluent flow just to the west of the cyclone center. There was no evidence of a secondary trough in this sector of the cyclone. A small-amplitude mid-tropospheric trough over Arizona and New Mexico was located too far from the cyclone center to be regarded as a mechanism responsible for the cloud and precipitation area over Minnesota and Iowa. Two other important characteristics of the wind field were readily identified over southeastern Ohio and northern Oklahoma where pronounced diffluent and confluent flow were present, respectively. The relevance of these features will be discussed in Section 4.

A satellite picture for this case study shows an extensive layer of stratiform clouds west of the low

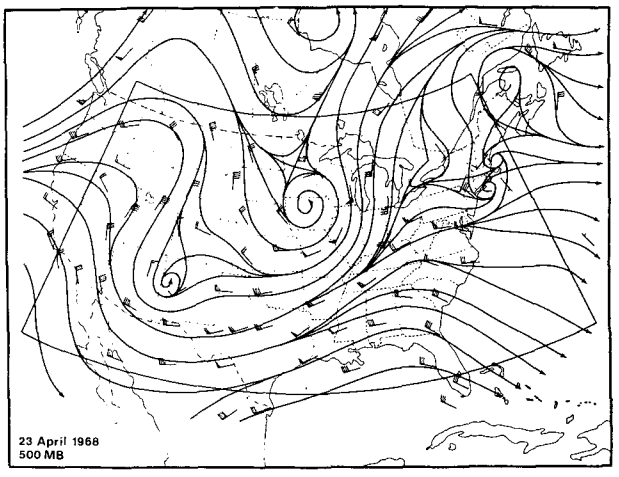

FIG. 5. Streamline analysis of the 500 mb level.

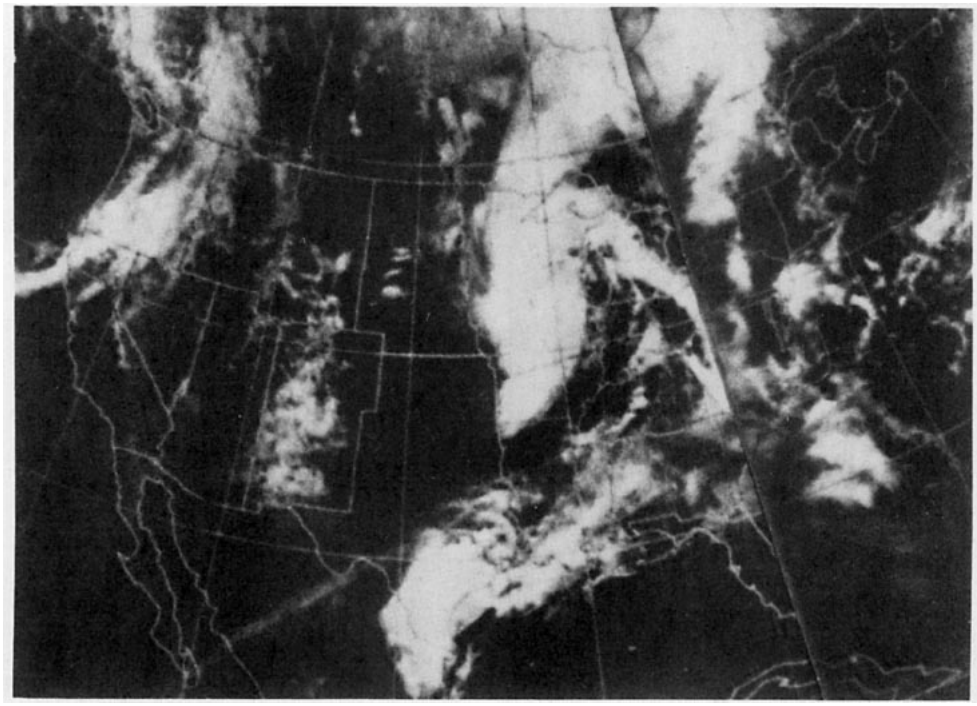

FIG. 6. ESSA 3 digitized picture at approximately 1715 GMT on April 1968.

center in Fig. 6. Convective cloud types predominated ahead of the cold front. The picture time was approximately 1715 GMT when the cyclone center was located over Wisconsin. Consequently, the cloud area behind the cyclone center in Fig. 6 was displaced northeast of its 1200 GMT location. Surface synoptic observations indicated stratus and stratocumulus overcast skies were present over most of Iowa and southern Minnesota at 1200 GMT.

The cloud structure associated with the 23 April 1968 storm is distinctly different from the more-often-observed deep occluded storms over oceans where convective clouds typically form to the west of the cyclone center in response to strong heating by a warm ocean surface and to instability associated with cyclonic vorticity at mid-tropospheric levels. This has been described by Petterssen *et al.* (1962) in a study of cyclones over the North Atlantic. GOES infrared imagery has shown convection extends through a deep layer and is often associated with secondary vorticity centers following the cyclone.

3. Numerical computations

To explain the mechanisms responsible for the cloud and precipitation fields for the 23 April 1968 cyclone, a multi-level nonlinear balanced model was employed. The physical mechanisms controlling the disturbance were investigated by computing the vertical motions with this model. Vertical motions arising from 13 forcing functions were partitioned according to the method developed by Krishnamurti (1968a).

The numerical computations involve solutions of three equations. These include a nonlinear system of partial differential equations that yield the vertical velocity ω from the omega equation, velocity potential χ from the mass continuity equation, and the stream-function tendency $\partial\psi/\partial t$ from the vorticity equation.

The omega equation used in this study was

$$\nabla^2\sigma\omega+f^2\frac{\partial^2\omega}{\partial p^2}=f\frac{\partial}{\partial p}J(\psi,\zeta_a)+\pi\nabla^2J(\psi,\theta)+f\frac{\partial}{\partial p}g\frac{\partial}{\partial p}\left(\frac{\partial\tau_y}{\partial x}-\frac{\partial\tau_x}{\partial y}\right)-2\frac{\partial}{\partial t}\frac{\partial}{\partial p}J\left(\frac{\partial\psi}{\partial x},\frac{\partial\psi}{\partial y}\right)-f\frac{\partial}{\partial p}(\zeta\nabla^2\chi)-\frac{R}{c_pp}\nabla^2H_L-\frac{R}{c_pp}\nabla^2H_s+f\frac{\partial}{\partial p}\left(\omega\frac{\partial}{\partial p}\nabla^2\psi\right)+f\frac{\partial}{\partial p}\left(\nabla\omega\cdot\nabla\frac{\partial\psi}{\partial p}\right)-f\frac{\partial}{\partial p}(\nabla\chi\cdot\nabla\zeta_a)-\pi\nabla^2(\nabla\chi\cdot\nabla\theta)-\beta\frac{\partial}{\partial p}\frac{\partial}{\partial y}\frac{\partial\psi}{\partial t}. \quad (1)$$

The symbols used in Eq. (1) are defined in the Appendix. Interpretation of each forcing function was described in detail by Krishnamurti (1968a) and those of particular interest in this study will be discussed in the next section. A numerical solution for ω was obtained by applying a three-dimensional relaxation procedure to Eq. (1) and using the continuity and vorticity equation to solve for χ and $\partial\psi/\partial t$.

Specific attention should be given to two forcing functions in Eq. (1) that are relevant to this study. First, the effects of latent heat are parameterized as convective and nonconvective types of latent heat release and are discussed in detail by Krishnamurti and Moxim (1971). Second, it should be noted that frictional stress terms in Eq. (1) are defined at the 1000 mb level according to the relations

$$\tau_x = C_D \rho u (u^2+v^2)^{\frac{1}{2}} \quad \text{and} \quad \tau_y = C_D \rho v (u^2+v^2)^{\frac{1}{2}}, \quad (2)$$

where C_D is a nondimensional drag coefficient assumed to be equal to a constant value of 2.5×10^{-3} over the grid domain. Terrain-induced vertical motions were included into the numerical solution by treating orographic effects as an external forcing function to solve for omega according to Krishnamurti (1968a). Terrain heights at 1° grid intervals were used from a report by Berkofsky and Bertoni (1960).

The forcing function due to sensible heat transfer was neglected because stable lapse rates prevailed west of the cyclone center over Minnesota and Iowa. Under these conditions, for the lower troposphere, heat transfer from the underlying surface is usually very small. Also, it was assumed that heat transfer from the Great Lakes was not an important factor in this April storm because the lake temperatures were colder than the overlying air and the cyclone center was too far west of the Great Lakes. It is only during a strong cold air outbreak in the autumn or early winter that the Great Lakes are important in this respect (Neralla and Danard, 1975).

The numerical computations were carried out on a 27×15 horizontal grid domain with a 2° mesh size as shown in Fig. 7. The region of study was chosen to be centered over the cyclone center in order to minimize boundary effects. Subjective analyses of geopotential heights and relative humidity provided input data for the sea level, 850, 700, 500, 300 and 200 mb surfaces.

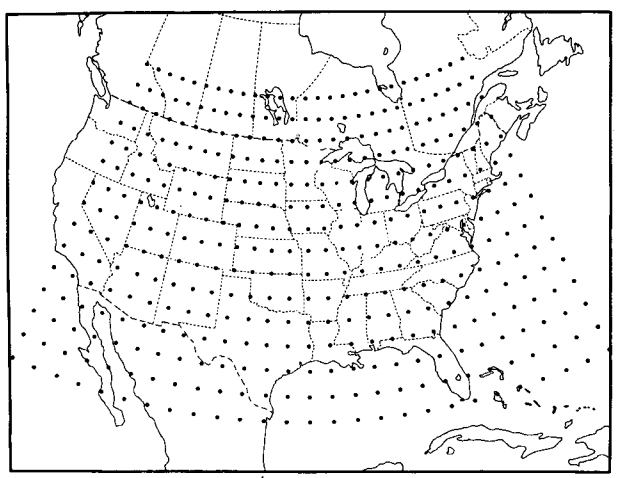

FIG. 7. Horizontal grid used in the numerical computations over a 27×15 domain with a 2° mesh size.

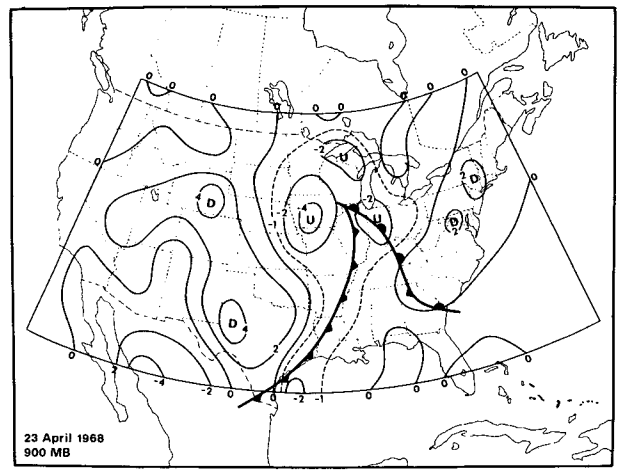

FIG. 8. Total vertical motion field at 900 mb. Isopleth interval is 2 μb s^{-1}.

Radar summaries and ATS III film loops were used to supplement conventional data in a subjective analysis of the relative humidity field, especially to interpolate moisture gradients between radiosonde stations at mid-tropospheric levels. The 200 mb relative humidities were assumed to be negligible.

4. Discussion of the results

The results of the numerical computations of the vertical motion field at four pressure surfaces are depicted in Figs. 8–11. Comparisons of the omega fields portrayed in these figures with the precipitation patterns schematically illustrated in Fig. 3 showed good agreement. In general, the omega values associated with this cyclone were less than those typically found with other, more intense extratropical systems (i.e., Krishnamurti, 1968b). Largest omega values ranged from -5 to $+6$ μb s^{-1} and exhibited a typical cellular configuration with areas of ascent ahead of and subsi-

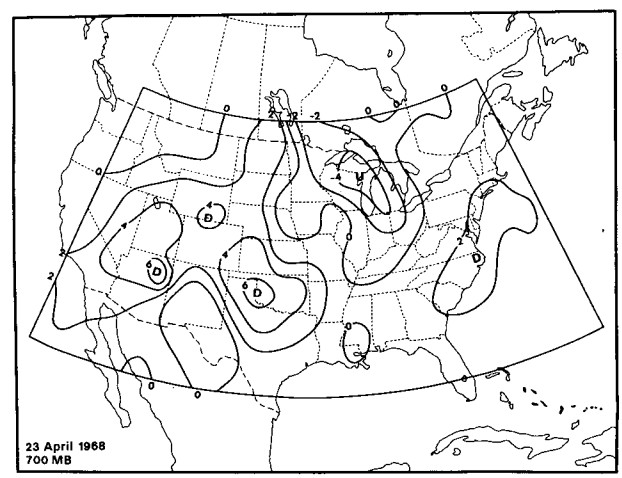

FIG. 9. As in Fig. 8 except for 700 mb.

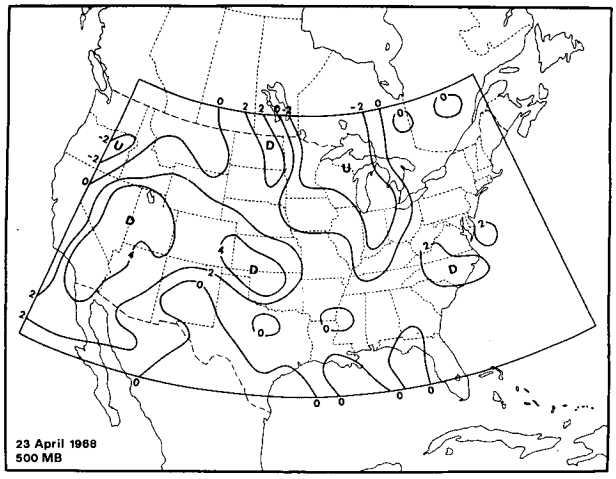

FIG. 10. As in Fig. 8 except for 500 mb.

dence behind the cyclone. Careful examination of the details in the vertical motion field revealed some interesting asymmetric features around the cyclone center and provided considerable insight into the role of the complex physical mechanisms involved.

a. Vertical motions west of the cyclone center

An area of strong ascending motions at 900 mb was located in the rear quadrant of the cyclone and was associated with the low-level clouds and light precipitation over Minnesota and Iowa. Omega values at the 900 mb level over Iowa, as shown in Fig. 8, were of the order of $-4\,\mu b\ s^{-1}$. This corresponds to approximately 3.5 cm s^{-1} rising motions. Omega values increased with height from negative to positive (i.e., from rising to sinking motion) in this sector of the storm and weak subsidence was present at 300 mb (Fig. 11). It is also interesting to note that the western edge of the precipitation area closely corresponded to the zero omega isopleth at 700 mb (Fig. 9).

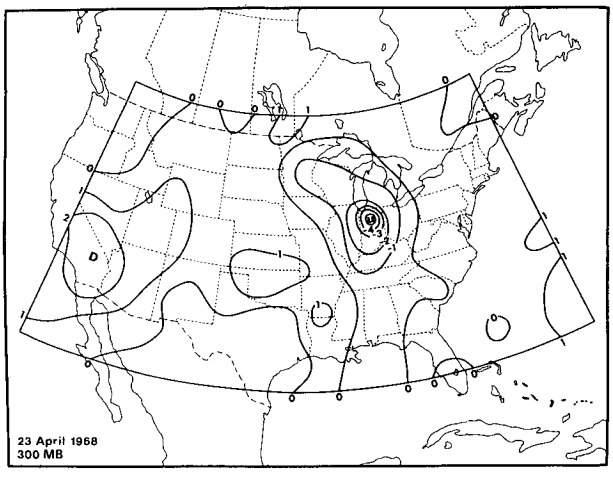

FIG. 11. As in Fig. 8 except for 300 mb.

Further west of the cyclone, rising motions were replaced by subsidence at all levels. Strongest sinking motions within the lower troposphere occurred in the high pressure center over Wyoming and throughout the ridge extending southwestward into Oklahoma. A wedge of sinking motion at 700 mb spiraled into the southwest quadrant of the cyclone center from a core of maximum downward motion of $6\,\mu b\ s^{-1}$ over western Oklahoma. This wedge may have been an important factor in determining the southern extent of the area of light precipitation and low level clouds over Iowa.

b. Vertical motions east of the cyclone center

The vertical motion field in this portion of the cyclone contrasted to the western half of the system. Strong ascending motions extended throughout the troposphere. This is illustrated in a vertical cross section extending east-west through the storm center along 41°N. Near 86°W a core of large omega values were present with intensities in excess of $-3\,\mu b\ s^{-1}$ at 900 mb and $-5\,\mu b\ s^{-1}$ at 300 mb. The strong upward motions were expected because the cloud field in this sector of the cyclone was characterized by convective and multi-layered clouds, as compared to the stratiform clouds near 41°N, 94°W where strong, rising motions were confined to stable lower levels.

c. Partitioned vertical motions

Contributions by each of the forcing functions defined in Eq. (1) provided information about the physical mechanisms at four pressure levels that can be primarily attributed to the ascending motions within the cloud and precipitation fields. Relative magnitudes of omega values produced by the individual terms are listed in Table 1 for two grid point locations. Both points were selected from the cross section shown in Fig. 12 and represent the areas of maximum rising motions to the west (41°N, 94°W) and east (41°N, 86°W) of the cyclone center, respectively.

It is readily apparent from the result given in Table 1 that the vertical velocity contributions were dominated by four terms in Eq. (1). These include thermal and vorticity mechanisms, frictional effects and latent heat release. Each of these terms produced rising motion intensities greater than $-2\,\mu b\ s^{-1}$. Contributions by other mechanisms were generally less than $\pm 0.5\,\mu b\ s^{-1}$ and tended to cancel each other.

Frictional stresses determined most of the rising motions at 900 mb and was the largest of all terms to the west of the cyclone center (41°N, 94°W) where its contribution amounted to $-5.31\,\mu b\ s^{-1}$. This maximum omega value was associated with pronounced low-level cyclonic inflow and therefore favored low-level cloud development. Less intense rising motions on the east side of the cyclone were attributed to the cyclonic wind shear across the warm front. The frictional effects at

TABLE 1. Contributions to the total omega values by 13 partitioned vertical velocities defined in Eq. (1). Data were selected from two grid points in Fig. 11 and are listed for four pressure levels. Units are μb s^{-1}.

Forcing function	Symbol	Vertical motions (μb s^{-1}) 41°N, 94°W 900 mb	700 mb	500 mb	300 mb	41°N, 86°W 900 mb	700 mb	500 mb	300 mb
Differential vorticity advection by nondivergent part of wind	$f\frac{\partial}{\partial p}J(\psi,\zeta_a)$	0.21	−0.25	−0.92	−0.23	−0.58	−2.59	−1.05	−0.76
Laplacian of thermal advection by nondivergent part of wind	$\pi\nabla^2 J(\psi,\theta)$	−2.06	0.35	1.15	0.72	−0.63	0.57	−2.79	−2.75
Differential deformation	$-2\frac{\partial}{\partial t}\frac{\partial}{\partial p}J\left(\frac{\partial\psi}{\partial x},\frac{\partial\psi}{\partial y}\right)$	0.29	0.46	−0.05	0.02	0.19	0.64	0.90	0.01
Differential divergence	$-f\frac{\partial}{\partial p}(\zeta\nabla^2\chi)$	1.24	0.14	0.09	0.06	1.10	0.30	0.21	0.36
Frictional stresses at surface	$f\frac{\partial}{\partial p}g\frac{\partial}{\partial p}\left(\frac{\partial\tau_y}{\partial x}-\frac{\partial\tau_x}{\partial y}\right)$	−5.31	−1.10	−0.50	−0.01	−2.48	−0.90	−0.51	−0.16
Latent heat release	$-\frac{R}{c_p p}\nabla^2 H_L$	−0.11	−0.29	−1.30	−0.30	−0.32	−1.20	−0.57	−2.55
Differential vertical advection of vorticity	$f\frac{\partial}{\partial p}\left(\omega\frac{\partial}{\partial p}\nabla^2\psi\right)$	−0.21	−0.03	0.09	0.08	−0.19	0.03	0.20	0.17
Differential twisting effects	$f\frac{\partial}{\partial p}\left(\nabla\omega\cdot\nabla\frac{\partial\psi}{\partial p}\right)$	0.01	−0.02	0.01	−0.03	0.11	−0.07	−0.12	−0.02
Differential advection of vorticity by divergent part of wind	$-f\frac{\partial}{\partial p}(\nabla\chi\cdot\nabla\zeta_a)$	−0.65	−0.15	−0.02	−0.02	−0.15	−0.15	−0.17	−0.18
Laplacian of thermal advection by divergent part of wind	$-\pi\nabla^2(\nabla\chi\cdot\nabla\theta)$	1.42	−0.14	−0.16	−0.27	−0.29	0.31	0.24	0.72
Beta effect	$-\beta\frac{\partial}{\partial p}\frac{\partial}{\partial y}\frac{\partial\psi}{\partial t}$	0.01	0.00	0.00	−0.01	−0.02	−0.01	−0.02	0.00
Sensible heat transfer at lower boundary	$-\frac{R}{c_p p}\nabla^2 H_s$	0.00	0.00	0.00	0.00	0.00	0.00	0.00	0.00
Surface terrain effect	$-\frac{gp}{RT}[J(\psi,h)-\nabla\chi\cdot\nabla h]$	0.00	0.00	0.00	0.00	−0.29	0.00	0.00	0.00
Total		−5.16	−1.03	−1.61	0.01	−3.55	−3.07	−3.68	−5.16

41°N, 86°W together with low-level moisture convergence were important in producing convective processes and generating ascending motions which were intensified by latent heat release at higher levels.

In another study, frictionally induced vertical motions were computed for a wintertime cyclone over the Great Lakes Region by Jarvis and Agnew (1970). They found reasonable agreement between vertical motions and clouds at low levels when only terrain and frictional effects were considered. However, their low-level vertical motion field was somewhat weaker than the one computed here. This is surprising in view of the fact that Jarvis and Agnew (1970) used a smaller grid spacing. However, in their investigation the geostrophic approximation was employed while this study was more dynamically complete with both the divergent and nondivergent parts of the flow included in the computations. Another reason may be found in differences between the synoptic systems investigated in each study.

The Laplacian of thermal advection and differential vorticity advection by the nondivergent flow contributed to rising motions primarily in the upper troposphere ahead of the cyclone and sinking motions immediately behind the cold front at low levels. Behind the cyclone (near 41°N, 96°W) the contribution to vertical motion by increasing vorticity advection with height was offset by the contribution from cold air advection. A similar result was obtained by Krishnamurti (1968b). Fig. 13 shows the combined effect of these two forcing functions at 900 mb. It can be seen that contributions to vertical velocity at this level in the vicinity of the low center were very small. This suggests that the effects of warm air advection at 850 mb, that sometimes develop west and northwest of

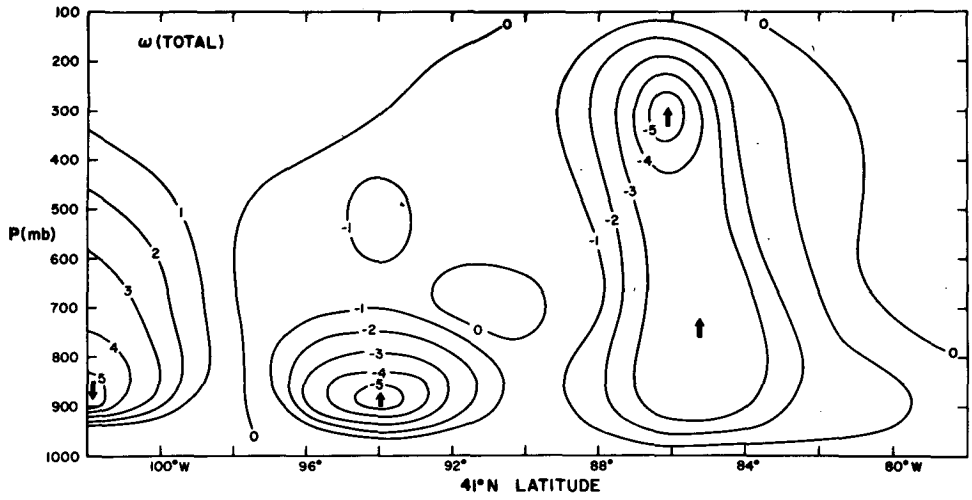

FIG. 12. East-west vertical cross section of vertical motions through the cyclone and along 41°N latitude. Units are the same as in Fig. 8.

occluded cyclones in the upper Midwest and are associated with a "wrap-around" of precipitation, were much weaker than frictional effects.

The latent heat contribution west of the storm in the stable air was of secondary importance compared to frictional stresses and thermal effects. However, east of the cyclone, especially within the conditionally unstable air over Indiana and western Ohio, the latent heat effect was comparable to the Laplacian of thermal advection. Rising motion due to convective type of latent heat release at 300 mb occurred within an elongated north-south pattern. Computations in the convective parameterization technique of large-scale moisture convergence in the boundary layer and conditionally unstable air throughout the troposphere explained the maximum value of $-2.55\ \mu b\ s^{-1}$ at 41°N, 86°W. This strong core of ascending motion nearly coincided with a line of thunderstorms that was reported on the radar summary at 1135 GMT (Fig. 3) and seemed reasonable for conditions with deep cumulus convection with little entrainment. Precipitation rates associated with these thunderstorms amounted to more than 0.20 inch h^{-1}. No attempts were made to calculate precipitation rates because the diagnostic equations provided only instantaneous values of computed parameters. Moreover, comparisons with observed precipitation amounts were limited by the rapid movement of the storm as well as the sampling problems of the hourly raingage network whenever convective systems were present. It should be noted that several hours later, the convective activity intensified and produced tornadoes over Ohio (Sikdar *et al.*, 1970). The clouds and weather in this sector of the cyclone were in marked contrast to the low-level clouds, light precipitation and stable type of latent heat release on the west side of the storm center.

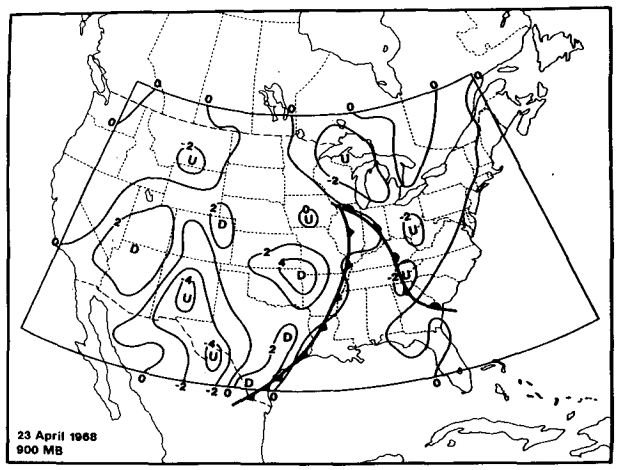

FIG. 13. Vertical motion field at 900 mb due to differential vorticity advection and the Laplacian of thermal advection by the nondivergent part of the wind.

5. Concluding remarks

The numerical model employed in this study was a useful tool in examining the physical mechanisms that produced the clouds and weather associated with a mid-latitude cyclone, particularly in the cold air sector to the west of the low pressure center. This study illustrates how frictional stresses may influence the distribution of clouds and weather in a cyclone and together with latent heat release may substantially modify the vertical motion field, which is usually dominated by vorticity and thermal contributions.

Results of this case study indicated that surface friction was the primary cause of low-level clouds and precipitation west of the cyclone center. This mechanism appears to be important in the absence of secondary upper level trough mechanisms or intense heating from the underlying surface.

The significance of low-level ascending motions here

suggests that vertical motions at the top of a moist boundary layer may be a useful forecast parameter for low-level clouds and precipitation for this type of synoptic situation. It is suggested that the nondivergent streamfunction and velocity potential could be obtained from surface synoptic observations and used operationally to compute vertical velocities at the top of the boundary layer. It may be possible to carry out such a technique at a frequency greater than twice (0000 and 1200 GMT) per day over a limited grid domain at local forecast offices that are equipped with minicomputer facilities. The potential for improving forecasts and the operational feasibility of this problem needs to be investigated further.

Acknowledgment. The author would like to acknowledge the helpful comments by the reviewers.

APPENDIX

List of Symbols

C_D	nondimensional drag coefficient
f	Coriolis parameter
h	surface terrain height
H_L	latent heating function
H_s	sensible heating function
J	Jacobian operator
L	latent heat coefficient
u	zonal component of total balanced wind
v	meridional component of total balanced wind
β	meridional variation of Coriolis parameter
ζ	relative vorticity
ζ_a	absolute vorticity
θ	potential temperature
π	$RT/p\theta$
σ	static stability
τ_x, τ_y	frictional stresses
ϕ	geopotential
χ	velocity potential
ψ	streamfunction
ω	vertical velocity in pressure coordinates

REFERENCES

Anderson, R. K., and N. F. Veltishchev, Eds., 1973: The use of satellite pictures in weather analysis and forecasting. Tech. Note No. 124, World Meteorological Organization, Geneva, 275 pp.

Astling, E. G., 1976: Low-level clouds and precipitation associated with mid-latitude cyclones. *Preprints Sixth Conf. Weather Forecasting and Analysis*, Albany, Amer. Meteor. Soc., 305–309.

Berkofsky, L., and E. A. Bertoni, 1960: Topographical charts at one degree intersections for the entire earth. Rep. No. 42, Geophysical Research Directorate, AFCRL, Bedford, Mass., 28 pp.

Colucci, S. J., 1976: Winter cyclone frequencies over the eastern United States and adjacent western Atlantic. *Preprints Sixth Conf. Weather Forecasting and Analysis*, Albany, Amer. Meteor. Soc., 273–277.

Jarvis, E. C., and T. Agnew, 1970: A note on the computation of terrain and frictionally induced vertical motions. *J. Appl. Meteor.*, **9**, 942–946.

Krishnamurti, T. N., 1968a: A diagnostic balance model for studies of weather systems of low and high latitudes, Rossby number less than 1. *Mon. Wea. Rev.*, **96**, 197–207.

——, 1968b: A study of a developing wave cyclone. *Mon. Wea. Rev.*, **96**, 208–217.

——, and W. Moxim, 1971: On parameterization of convective and nonconvective latent heat release. *J. Appl. Meteor.*, **10**, 3–13.

Neralla, V. R., and M. B. Danard, 1975: Incorporation of parameterized convection in the synoptic study of large scale effects of the Great Lakes. *Mon. Wea. Rev.*, **103**, 388–405.

Petterssen, S., D. L. Bradbury and K. Pedersen, 1962: The Norwegian cyclone models in relation to heat and cold sources. *Geofys. Publ.*, **24**, 243–280.

Sikdar, D. N., V. E. Suomi and C. E. Anderson, 1970: Convective transport of mass and energy in severe storms over the United States—an estimate from a geostationary satellite. *Tellus*, **22**, 521–532.